Electron-impact excitation and ionization of molecular and liquid water using a pseudocontinuum method

Anthony Ferté,[1,*] Robin Santra,[1,2,3,†] and Ludger Inhester[1,2,‡]

[1]*Center for Free-Electron Laser Science CFEL, Deutsches Elektronen-Synchrotron DESY, Hamburg, Germany*
[2]*Hamburg Centre for Ultrafast Imaging, University of Hamburg, Hamburg, Germany*
[3]*Department of Physics, University of Hamburg, Hamburg, Germany*

(Received 15 December 2025; accepted 5 August 2026; published 26 August 2026)

We present an *ab initio* framework for computing inelastic electron scattering (IES) on isolated molecules and in condensed phases, focusing on liquid water as a prototypical target. Our method employs a pseudocontinuum treatment for electron-impact ionization. The scattered projectile is described by a plane wave, while the final states of the target, including the excited or ejected electron, are expanded in a square-integrable basis. This approach naturally describes the transition between the excitation and ionization regimes and enables molecular-hole-resolved IES cross sections to be extracted within a standard quantum-chemistry framework. For isolated water molecules, the computed IES cross sections agree with available experimental data. For liquid water, our calculations show that solvation has a small effect on the total IES cross section. We see, however, that the liquid environment leads to a substantial enhancement of electron-impact-induced ionization and a corresponding reduction of electron-impact-induced excitation. We discuss the total and hole-resolved single differential cross sections, offering a complete molecular picture of IES and paving the way toward a detailed simulation of radiation-damage formation in water.

DOI: 10.1103/h7g3-r5s3

I. INTRODUCTION

Inelastic electron scattering (IES) is a crucial process through which electrons propagating in a medium deliver energy into surrounding molecules via collision-induced excitations and ionizations. Developing an appropriate description of IES and its effect on the molecular target is thus of utmost importance for understanding the behavior of a condensed-phase system subjected to ionizing radiation. In particular, fully characterizing the state of the molecules in which energy is deposited is key to understanding how IES leads to the occurrence of radiation damage. Recently, probing the ultrafast collisional ionization dynamics became accessible through x-ray pump/x-ray probe experiments with subfemtosecond resolution, employing all-x-ray attosecond transient absorption spectroscopy, a.k.a. AXATAS [1]. In order to interpret how the collisional ionization dynamics imprint signatures on the recorded absorption spectrum, an accurate modeling of the involved IES processes with a focus on condensed phases is required.

Theoretical methods to compute IES cross sections (CSs), however, were so far largely focused on isolated atoms and molecules. At very high collision energies, IES can be fairly well understood without considering intricate details of the electronic structure of the target. Thus, properties of IES were often computed using semiempirical approaches [2–6] or extrapolated from experimental data and optical properties [7–12]. However, such methods remain limited by their semiempirical character, by the quality and availability of the required parameters, and leave aside information regarding the final state of the target. In contrast, at lower collision energy, IES becomes increasingly sensitive to the properties of the involved atomic or molecular states [10,13,14]. In this regime, characterizing IES requires *ab initio* calculation accurately describing the interaction between the projectile and the electronic structure of the target.

While it has been proposed that IES could be treated in the framework of time-dependent density-functional theory [15], most *ab initio* strategies rely on wave-function approaches and use explicit continuum waves to describe both scattered projectile and ejected target electron [16–19]. The methods focus on electron-impact-induced ionization and mostly differ from one another by the type of continuum wave used for either of the free electrons (plane waves, Coulomb waves, or distorted waves) and by the wave-function *ansatz* used to describe bound electrons. These approaches naturally give access to high-order derivatives of the electron-impact-induced ionization cross section and are well suited to describe collisions when secondary electrons are ejected with sufficiently large momentum. For condensed-phase systems, when the excited or ejected target electron carries only a small amount of momentum, it considerably interacts with the chemical environment and thus a plane-wave description becomes

*Contact author: anthony.ferte@desy.de
†Contact author: robin.santra@desy.de
‡Contact author: ludger.inhester@desy.de

unsuitable. Accordingly, simulating IES in liquid water remains a theoretical challenge and most available approaches are not really designed for describing IES in condensed phase and mostly focus on gas-phase experiments [4,6,15–17,19,20].

Concrete differences in the IES between gas-phase and liquid-phase water may be expected because the electronic structure of a water molecule in a liquid environment is altered compared to the one of an isolated molecule. For example, ionization energies are considerably different [21]. Moreover, excited states and the low-energy continuum are strongly influenced by the chemical environment [22]. Thus, differences in the IES cross section should appear in the intermediate collision-energy range, where details of the electronic structure of the target strongly influence the collisional process. In water, this becomes relevant at a collision energy below 250 eV, i.e., in the pertinent energy range for the appearance of biological radiation damage [14,23]. Only few attempts were made to describe IES in liquid water within an *ab initio* framework. In particular, de Sanctis *et al.* [24–26] employed a one-active-electron model for collisional ionization based on a Coulomb-wave description for the ejected electron, whereas Koval *et al.* [14] used an approach based on linear-response time-dependent density-functional theory with a local-density-approximation-type functional to compute the electron-energy loss function.

Pseudocontinuum methods offer an interesting alternative in this context. Within such a framework, only the projectile is explicitly described by a plane wave, whereas the final state of the target (including the excited or ejected electron) is described by discrete eigenstates of the Hamiltonian operator projected in a finite square-integrable (L^2) basis. This approach is naturally well suited for describing the transition between the excitation regime and the ionization regime. However, because it only yields a discretized approximation of the ionization continua, postprocessing such as utilizing the moment-theory-based Stieltjes-imaging procedure [27,28] is required to recover physically relevant information past the ionization threshold. At the moment, usage of methods relying on pseudocontinuum states to describe inelastic scattering remains scarce and limited to atoms [29] and small systems [30].

In this paper, we present a computational strategy relying on a pseudocontinuum description of electron-impact ionization to describe IES at both low and high impact energy and momentum transfer. We show that when using a basis set suitable to describe pseudocontinuum states, our approach appropriately describes the ionization regime while bound excitations are naturally well described. Our approach offers a straightforward way to extract cross sections for specific excitation/ionization channels and thus to build a picture of IES with an emphasis on the molecular aspects of the target rather than on the projectile. We apply this method to investigate IES in liquid water, i.e., the most essential solvent in biological systems, for which IES is critical to the occurrence of radiation damage, and compare our results with those we obtain for an isolated water molecule. Our simulations provide a complete molecular picture of the effects of electron impact in liquid water. The obtained partial cross sections are the missing piece to allow to fully model the formation of radiation damage created through cascades of electron collisions in water and the appearance of the corresponding spectroscopic signatures.

The paper is organized as follows: In Sec. II, we present the theoretical and computational aspects of our method. We break down the approximations made to derive the IES cross sections (Sec. II A) and make explicit the practical aspects of our method, i.e., the description of liquid water, the treatment of the electronic structure, and the reconstruction procedure to describe ionization continua from pseudocontinuum transitions (Sec. II B). In Sec. III, we discuss the results for the IES cross section for isolated water molecules (Sec. III A) and liquid water (Sec. III B). Finally, in Sec. IV, we summarize our conclusions.

II. THEORY AND METHOD

A. Inelastic electron scattering: Total and differential cross sections

In the following, we focus on electronic processes in the target and neglect nonelectronic processes such as vibrational and rotational excitations that naturally become relevant at very low collision energy [9,13,31]. Moreover, we consider a regime where nuclear excitations are irrelevant, so the inelastic interaction of the projectile electron involves the bound electrons in a target molecule.

We employ atomic units throughout this paper, in which $\hbar = m_e = |e| = 1$. Employing first-order perturbation theory, the IES double-differential cross section, i.e., the derivative of the IES cross section σ with respect to the energy ε_F and direction Ω of the scattered projectile electron in a finite volume V and parametrized by its incoming momentum $\mathbf{k}_\mathrm{I}$ and spin Σ_I, is [29,32]

$$\frac{d^2\sigma(\mathbf{k}_\mathrm{I},\Sigma_\mathrm{I})}{d\Omega\, d\varepsilon_\mathrm{F}} = \frac{V^2|\mathbf{k}_\mathrm{F}|}{4\pi^2|\mathbf{k}_\mathrm{I}|}\sum_\mathrm{F}\!\!\!\!\!\!\int \left|\left\langle\Psi_\mathrm{F}^\mathrm{tot}\middle|\hat{W}_\mathrm{ee}\middle|\Psi_\mathrm{I}^\mathrm{tot}\right\rangle\right|^2 \times\ \delta(E_\mathrm{I}-E_\mathrm{F}+\varepsilon_\mathrm{I}-\varepsilon_\mathrm{F}), \tag{1}$$

with $|\Psi_\mathrm{I}^\mathrm{tot}\rangle = |\Psi_\mathrm{I},\phi_\mathrm{I}\rangle$ being the initial electronic state of the system with the molecular target in the state $|\Psi_\mathrm{I}\rangle$ with energy E_I and an incoming projectile electron in state $|\phi_\mathrm{I}\rangle$ with spin Σ_I, asymptotic momentum $\mathbf{k}_\mathrm{I}$, and energy $\varepsilon_\mathrm{I} = \mathbf{k}_\mathrm{I}^2/2$. In Eq. (1), $|\Psi_\mathrm{F}^\mathrm{tot}\rangle = |\Psi_\mathrm{F},\phi_\mathrm{F}\rangle$ is the final state of the system with the molecular target in the state $|\Psi_\mathrm{F}\rangle$ with energy $E_\mathrm{F} \neq E_\mathrm{I}$ and an outgoing electron in state $|\phi_\mathrm{F}\rangle$ with spin Σ_F, asymptotic momentum $\mathbf{k}_\mathrm{F}$, and energy $\varepsilon_\mathrm{F} = \mathbf{k}_\mathrm{F}^2/2$. The combined sum and integral symbol indicates that the summation runs over both discrete (bound) and continuum (ionized) final states $|\Psi_\mathrm{F}\rangle$. The electronic Coulomb operator $\hat{W}_\mathrm{ee}$ describes the electron-electron interaction. The Coulomb-matrix element in Eq. (1) leads to two contributions, a direct term,

$$\langle\Psi_\mathrm{F}|\hat{a}_j^\dagger\hat{a}_i|\Psi_\mathrm{I}\rangle\ \langle u_j,\phi_\mathrm{F}\,|\,u_i,\phi_\mathrm{I}\rangle, \tag{2}$$

and an exchange term,

$$-\langle\Psi_\mathrm{F}|\hat{a}_j^\dagger\hat{a}_i|\Psi_\mathrm{I}\rangle\ \langle\phi_\mathrm{F},u_j\,|\,u_i,\phi_\mathrm{I}\rangle, \tag{3}$$

where $\hat{a}_j^\dagger$ and $\hat{a}_i$ are creation and annihilation operators that add and remove an electron in the one-electron state $|u_j\rangle$ with spin Σ_j and $|u_i\rangle$ with spin Σ_i, respectively. In Eqs. (2) and (3), we have used the common abbreviation for Coulomb

integrals,

$$\langle u_j, \phi_F \,|\, u_i, \phi_I\rangle = \delta_{\Sigma_j,\Sigma_i}\delta_{\Sigma_F,\Sigma_I} \iint d^3r_1 d^3r_2 \frac{1}{|\mathbf{r}_1 - \mathbf{r}_2|} \times u_j^*(\mathbf{r_1}) u_i(\mathbf{r_1}) \phi_F^*(\mathbf{r_2}) \phi_I(\mathbf{r_2}) \quad (4)$$

and

$$\langle \phi_F, u_j \,|\, u_i, \phi_I\rangle = \delta_{\Sigma_F,\Sigma_i}\delta_{\Sigma_j,\Sigma_I} \iint d^3r_1 d^3r_2 \frac{1}{|\mathbf{r}_1 - \mathbf{r}_2|} \times \phi_F^*(\mathbf{r_1}) u_i(\mathbf{r_1}) u_j^*(\mathbf{r_2}) \phi_I(\mathbf{r_2}), \quad (5)$$

where the Kronecker $\delta_{\Sigma_a,\Sigma_b}$ symbols are 1 if the electron spins Σ_a and Σ_b are equal, and 0 otherwise.

To evaluate the spatial part of the Coulomb integrals, we make use of the Born approximation, in which the projectile states are approximated by box-normalized plane waves,

$$\langle \mathbf{r}|\phi_I\rangle = \frac{e^{i\mathbf{k}_I\cdot\mathbf{r}}}{\sqrt{V}} \quad \text{and} \quad \langle \mathbf{r}|\phi_F\rangle = \frac{e^{i\mathbf{k}_F\cdot\mathbf{r}}}{\sqrt{V}}. \quad (6)$$

Within this framework and using Bethe's integral [33], one can rewrite the Coulomb integral in Eq. (4),

$$\langle u_j, \phi_F \,|\, u_i, \phi_I\rangle = \delta_{\Sigma_j,\Sigma_i}\delta_{\Sigma_F,\Sigma_I} \frac{1}{V}\frac{4\pi}{\mathbf{K}^2} \langle u_j \,|\, e^{i\mathbf{K}\cdot\mathbf{r}} \,|\, u_i\rangle, \quad (7)$$

with $\mathbf{K} = \mathbf{k}_I - \mathbf{k}_F$ the projectile momentum transferred during the collision. The factor $1/\mathbf{K}^2$ in the Coulomb-matrix element in Eq. (7) suppresses large momentum transfer in the inelastic scattering.

To apply a similar treatment to the Coulomb integral corresponding to the exchange term of Eq. (5), we first introduce the Fourier decomposition of the spatial part of the final states of the excited or ejected electron,

$$u_j(\mathbf{r}) = \int d^3k_j \, \tilde{u}_j(\mathbf{k}_j) \, e^{i\mathbf{k}_j\cdot\mathbf{r}}. \quad (8)$$

One can then rewrite

$$\begin{aligned}\langle \phi_F, u_j \,|\, u_i, \phi_I\rangle &= \int d^3k_j \tilde{u}_j^*(\mathbf{k}_j) \langle \phi_F, \mathbf{k}_j \,|\, u_i, \phi_I\rangle \\ &= \int d^3k_j \, \frac{1}{V}\frac{4\pi}{\mathbf{K}_j^2} \, \tilde{u}_j^*(\mathbf{k}_j) \langle \mathbf{k}_F \,|\, e^{i\mathbf{K}_j\cdot\mathbf{r}} \,|\, u_i\rangle \\ &\quad \times \delta_{\Sigma_F,\Sigma_i}\delta_{\Sigma_j,\Sigma_I}, \end{aligned} \quad (9)$$

where $\mathbf{K}_j = \mathbf{k}_I - \mathbf{k}_j$ now represents the momentum difference between the incoming projectile electron and the final plane-wave component, in which the target electron $u_j(\mathbf{r})$ is expanded.

It is important to realize that the factor $1/\mathbf{K}_j^2$ considerably suppresses the exchange contribution as long as $|\mathbf{k}_j| \ll |\mathbf{k}_I|$, which is the case when the direct term dominates, i.e., $\mathbf{k}_I \simeq \mathbf{k}_F$. Accordingly, exchange effects are expected to vanish when the outgoing electron has a largely different momentum than the excited or ejected electron. Furthermore, the direct term contributes only when the spin of the incident electron matches with the one of the outgoing electron, whereas the exchange term contributes only when the spin of the incident electron matches with the spin of the excited or ejected target electron u_j. Hence, in the specific scenario where the spin of the incident electron changes in the scattering process (spin flip), the exchange term is dominant. Such a spin flip must consequently also lead to a change of the spin state in the molecular target [34,35]. If no spin-flip scenario is considered, the exchange term becomes large when $\mathbf{k}_j \simeq \mathbf{k}_I$. Because of energy conservation, $\mathbf{k}_I - \mathbf{k}_F$ must be large, so the direct term is strongly suppressed. In this case, the ejected electron and the scattered electron change their roles. The interplay between the two terms routes back to the indistinguishability of the ejected and the scattered electron. This ambiguity is overcome by defining the scattered electron to be the one that has a similar momentum as the incoming projectile electron (i.e., the fast electron) and the excited or ejected electron as the one with low momentum contributions (i.e., the slow electron). Notably, considerations become more involved when the momentum of the projectile electron, and hence the momentum differences between outgoing and excited/ejected electrons, becomes eventually small.

For the remainder of the paper, we assume that the incoming projectile momentum $|\mathbf{k}_I|$ is sufficiently large, so that exchange effects can be neglected, as discussed above. Accordingly, we consider that the incoming electron has the same spin as the fast outgoing electron. Equation (1) can then be reformulated as [29,32]

$$\frac{d^2\sigma(\mathbf{k}_I)}{d\Omega\, d\varepsilon_F} = \frac{4}{|\mathbf{K}|^4}\frac{|\mathbf{k}_F|}{|\mathbf{k}_I|} \sum_F |\langle \Psi_F | e^{i\mathbf{K}\cdot\mathbf{r}} | \Psi_I\rangle|^2 \times \delta(E_I - E_F + \varepsilon_I - \varepsilon_F). \quad (10)$$

Integrating Eq. (10) over the outgoing direction of the scattered projectile Ω yields the single differential cross section (SDCS) $d\sigma(\mathbf{k}_I)/d\varepsilon_F$. As the derivative of the total cross section with respect to the outgoing projectile energy, or equivalently with respect to the energy transferred to the scattering target, the SDCS is the key quantity to investigate the molecular aspects of IES events.

B. Methodological framework

1. Sampling of water clusters

Molecular dynamics simulations were performed using the GROMACS software [36] version 2021.4 to generate and equilibrate a $3 \times 3 \times 3$ nm water cube containing 884 molecules with the extended simple point charge (SPC/E) optimized potential for liquid simulations (OPLS) force field [37,38]. This force field imposes freezing of the internal O–H bond distances and the H–O–H angle to improve the thermodynamic description of the ensemble. We employed the V-rescale thermostat [39] and the Parrinello-Rahman barostat [40–42]. For the dynamics, we used a 2-fs propagation time step and three-dimensional periodic boundary conditions. The particle mesh Ewald [43,44] scheme was used to compute the Coulomb interaction, while geometric rules were used to determine the Lennard-Jones parameters. First, an energy minimization was performed, followed by two consecutive 100 picoseconds (ps) equilibrations, first at constant particle number, volume, and temperature (NVT), and then at constant particle number, pressure, and temperature (NPT) at 300 K and 1 bar, respectively. Finally, an NPT production run was carried out for 1000 ps.

We then sampled 50 water clusters with an arbitrary orientation from the equilibrated water box. Each of them was generated by randomly selecting a water molecule and including all neighboring water molecules closer than 3.25 Å

(oxygen-oxygen distance) as its first solvation shell [45]. From this sampling, 19 pentamers, 15 hexamers, 11 tetramers, 4 heptamers, and 1 trimer were obtained, leading to an average cluster size of 5.2 water molecules. Among the leftover water molecules, those closer than 10 Å were included in our calculation as point charges, where we employed the partial-charge values defined by the force field.

2. *Electronic structure of the molecular target*

To simulate IES, the electronic structure of the molecular target was described at the configuration-interaction-singles (CIS) level and within the frozen-core approximation since, at the investigated collision energies, core excitations and ionizations only represent a negligible fraction of IES events. For the calculations involving water clusters, the IES was computed for the water molecule at the center of the cluster. To that end, in the CIS procedure, only excitations from the occupied orbitals localized on this central target molecule were allowed (without restricting the virtual space). In Appendix A, we show that this decoupling does not bias the description of IES, but instead prevents spurious contributions from the peripheral water molecules at the boundary of the cluster.

Molecular orbitals (MOs) were expanded in a standard atom-centered Gaussian-type orbital basis. To enhance the description of pseudocontinuum states, the basis was complemented with Kaufmann functions optimized to describe the ejected electron in the field of the cationic core [46,47]. If not otherwise stated, we used Pople's 6–31G* basis set [48–50] centered on each of the oxygen and hydrogen atoms, complemented by $10s$, $10p$, $10d$, and $5f$ Kaufmann basis functions centered on the oxygen atom of the central target molecule. In the following, we refer to such a complemented basis as "$\alpha s\beta p\gamma d\delta f$ + BASIS," when α s-type, β p-type, γ d-type, and δ f-type Kaufmann functions complement the usual BASIS.

For calculations involving an isolated water molecule, standard restricted Hartree-Fock (HF) orbitals were used. For liquid phase, i.e., water clusters, we used localized MOs obtained by first localizing the canonical HF orbitals of the water cluster using Boys' localization procedure [51,52]. We then partially "recanonicalized" the occupied orbitals localized on the target molecule at the center of the cluster by diagonalizing the subblock of the Fock matrix corresponding to these orbitals. This block recanonicalization procedure shares some aspects with the method proposed by Vuilleumier and co-workers [24–26,53] and is critical to recover localized MOs displaying symmetries similar to those of an isolated water molecule.

Importantly, this partial recanonicalization procedure only involves rotations among occupied MOs that are subsequently included in a CIS calculation. Therefore, this procedure does not affect the quality of the computed states. The use of MOs displaying relevant symmetries leads, however, to a more natural interpretation of the IES simulation. We found that despite the use of localized orbitals, our recanonicalization procedure allows the Fock matrix to retain a sufficiently diagonal-like character. This allows us to use the diagonal elements of the Fock matrix as Koopmans'-like estimations of the ionization potential (IP).

The electronic-structure and IES calculations were performed using a development version of XMOLECULE [54,55].

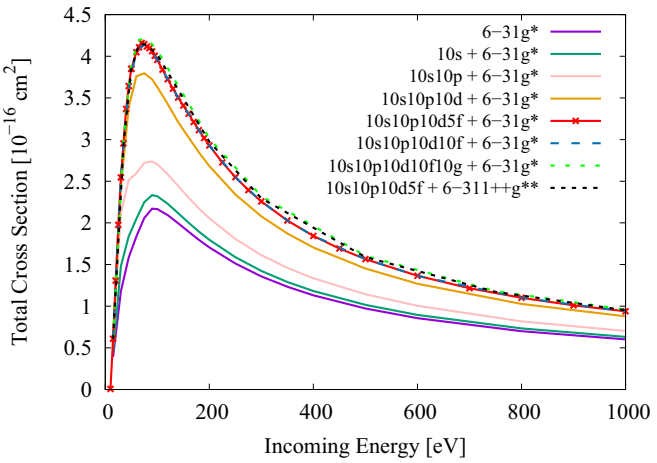

FIG. 1. Convergence of the calculated total IES CS for an isolated water molecule (optimized geometry) with respect to the size of the basis set. The initial projectile direction was taken along the z axis (see text).

In order to evaluate the IES, one has to compute matrix elements of the type

$$\int d^3r\, e^{i\mathbf{K}\cdot\mathbf{r}} \chi_\mu^*(\mathbf{r})\chi_\nu(\mathbf{r}), \tag{11}$$

where $\chi_\nu(\mathbf{r})$ and $\chi_\mu(\mathbf{r})$ are Gaussian basis functions. The computation of these matrix elements was implemented following the recursive relations given in Ref. [56].

To obtain SDCSs, integration over the scattering direction Ω was performed numerically using a tight Lebedev grid with $L = 101$ ($l_{\max} = 50$) [57] to resolve the characteristic highly directional behavior observed at high projectile velocity.

3. *Pseudocontinuum reconstruction*

Using standard quantum-chemistry methods to compute molecular electronic structure generally leads to a poor description of the continuous part of the electronic spectrum. This is because these approaches typically rely on a basis of bound-state-like square-integrable (L^2) functions. Such bases are unable to properly reproduce the nondecaying asymptotic behavior of unbound states. As a result, one only obtains discrete "pseudocontinuum" states approximating the true continuum within the constraint of the basis.

When considering an initial bound state of the target, it is expected that the matrix elements in Eq. (10) are only weakly influenced by the asymptotic behavior of the continuum wave functions. This important observation is the foundation for moment-theory methods, such as the Stieltjes-imaging procedure, which we employed to reconstruct the continuous part of spectra only using the discrete pseudocontinuum contributions [27,28].

III. RESULTS AND DISCUSSION

A. IES in gas-phase water

1. *Basis-set convergence*

We report in Fig. 1 the total IES CS obtained using our pseudocontinuum approach for an isolated water molecule at its optimized geometry as a function of the incoming projectile energy and for a series of basis sets. For these calculations,

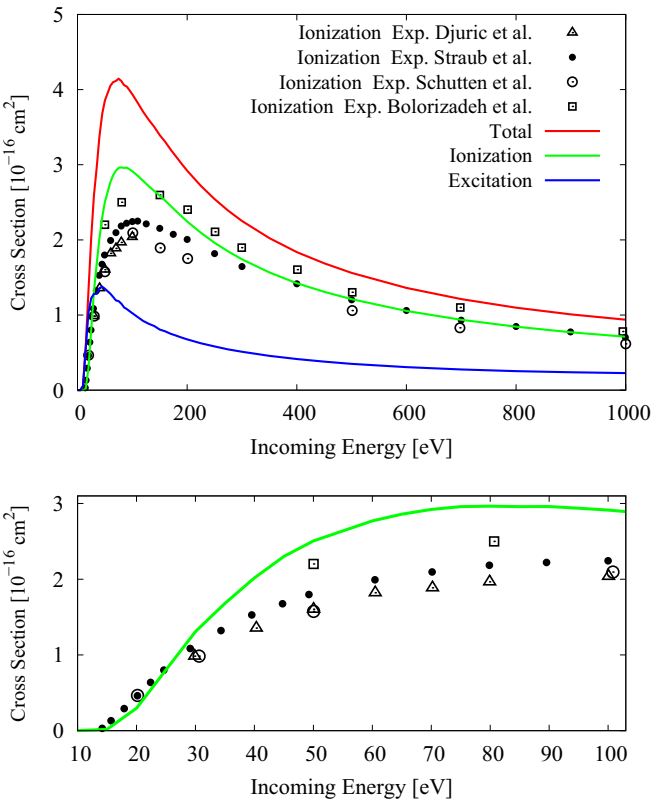

FIG. 2. (Top) Total IES cross section of an isolated water molecule (red) and its excitation (blue) and ionization (green) contributions at the optimized geometry, averaged over 100 randomly sampled initial projectile directions. Dots show measured electron-impact ionization CSs for gas-phase water taken from Refs. [58–61]. (Bottom) Ionization CSs in the sub-100 eV region.

the projectile direction was fixed along the C2-symmetry axis of the molecule that defines the z axis of the reference frame, the molecular plane defining the y-z plane. Regardless of the basis, the total IES CS rises quickly at low energy, reaches a maximum, and then gradually decays at high collision energy. A net increase in the computed IES CS is observed when functions of higher angular momentum are provided. It turns out that these high-angular-momentum Kaufmann functions are critical to describe pseudocontinuum states relevant for the electron-impact ionization. These observations are consistent with previous works on electron-impact ionization in water involving basis sets including functions of f-type symmetry [16,17,19]. We conclude that the $10s10p10d5f + 6{-}31G^*$ basis set provides sufficiently converged results. This basis set is thus used throughout the rest of the paper (see Appendix B for a convergence study on a water cluster).

2. *Electron-impact excitation and ionization*

To disentangle in our calculations electron-impact-induced excitation from collisional ionization, we assigned to each final CIS state a hole type identifying which of the $2a_1$, $1b_2$, $3a_1$, or $1b_2$ water orbitals bears the largest hole density. We then compared the excitation energy to the corresponding Koopmans' ionization potential to identify whether a transition contributes to the excitation or ionization CS. In Fig. 2, the total IES CS (red) as well as its excitation (blue) and ionization (green) components are presented as a function of the incoming projectile energy for an isolated water molecule. The results presented here have been obtained for the optimized geometry of the isolated water molecule, by averaging over 100 randomly sampled projectile directions. Experimental electron-impact ionization cross sections for gas-phase water [58–61] are shown for comparison.

Both components of the IES CS display similar characteristics as the total CS, i.e., a fast rise at low energy followed by a gradual decay. The collisional excitation CS starts rising at a slightly lower impact energy than its ionization counterpart, but ionization becomes dominant at energies above 40 eV. The collisional ionization CS reaches its maximum around 85 eV, whereas the total CS peaks at approximately 70 eV.

As one can see, our approach yields an ionization cross section that agrees very well with experimental values at collision energies higher than 400 eV, specifically the results of Straub *et al.* [61] (maximum deviation 2%). In this region, the measured ionization cross sections reported by Schutten *et al.* [58] are about 12% smaller and the ones reported by Bolorizadeh and Rudd [59] are about 15% larger. For lower incoming energies, the discrepancies between the calculated ionization cross sections as well as the discrepancies among the measured ionization cross sections are larger. In particular, our calculated IES ionization cross section has a maximum at slightly lower energy than the measured ones and overestimates the ionization cross section by up to 15%–40%, depending on the experimental data used as a reference. Factors that may play a role in causing this behavior are (1) artifacts due to the way we distinguish between excitation and ionization, in particular, the Koopmans'-like estimation used for the IPs, (2) limitations of the plane-wave description of the projectile (i.e., effects beyond the first Born approximation), and (3) the neglect of exchange contributions between scattered and ejected electrons in the final state [16,18]. While the latter two are expected to become more apparent at lower kinetic energy for the projectile electron, exchange effects are expected to be the dominant factor for the overestimation of the IES-induced-ionization-cross-section maximum. Indeed, the results presented in Ref. [18] for several diatomic molecules show on average a decrease of 30% for the ionization-cross-section peak due to the exchange effects, while the impact of employing a description beyond the plane-wave model for the ejected electron appears to be more limited.

3. *Structural fluctuations and molecular orientation*

We now discuss the effect of molecular structure and orientation on the IES CS. In Fig. 3, we report the IES total, ionization, and excitation cross sections of an isolated water molecule accounting for the orientation of the target at a fixed geometry by sampling 100 random initial projectile directions (red) and accounting for both the orientation and the structural fluctuations of the target (blue). As can be seen, the IES CSs vary only little when different orientations are considered. A slightly larger spread is observed when structural fluctuations are also considered. However, these variations of the total CS reach at most 15% for collision energies higher than 20 eV and become as low as 5% past the 200 eV mark. The averaged CSs

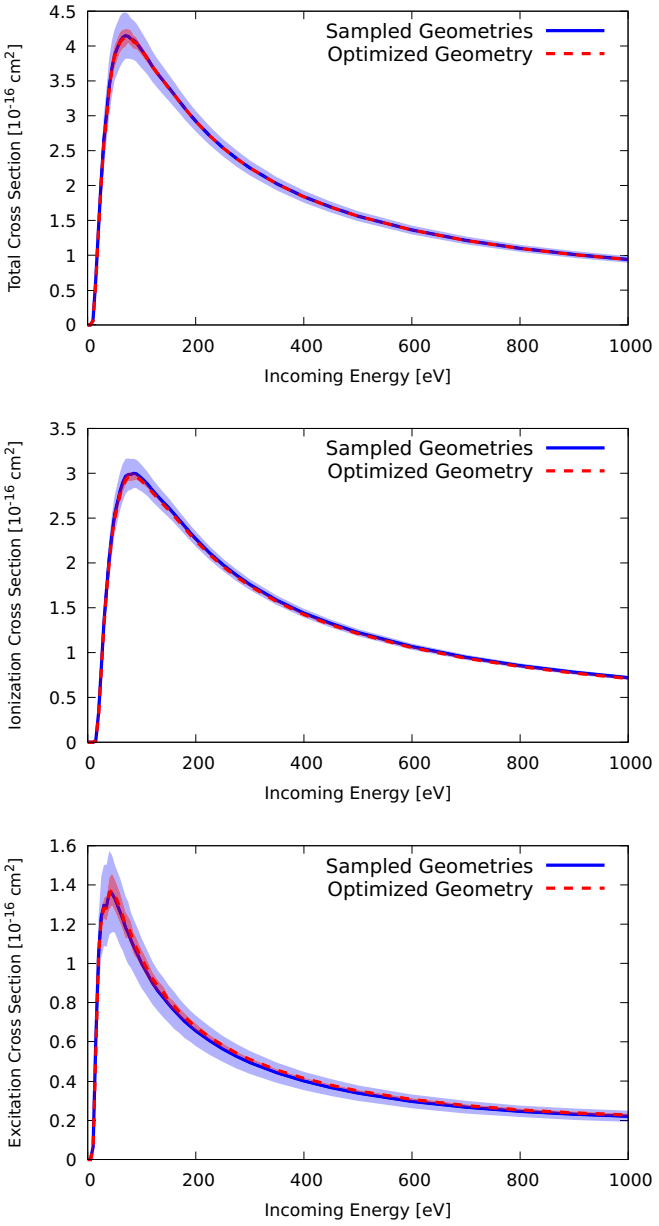

FIG. 3. Total IES cross section of an isolated water molecule target (top) and its ionization (middle) and excitation (bottom) contributions. (Red) Result obtained at the optimized isolated water geometry for 100 random projectile directions. (Blue) Result obtained for 200 geometries sampled from the ground-state Wigner distribution for random projectile directions. Shaded areas represent variation by up to one standard deviation.

are practically identical whether or not structural fluctuations are taken into account. For the present study, we therefore consider differences in the cross sections due to internal structural fluctuations to be negligible.

B. IES in liquid water

1. IES cross sections of sampled water clusters

Figure 4 shows the total IES CSs for the individual water clusters (gray) and when averaged over the full set (red). Here, the arbitrary orientation of the individual clusters

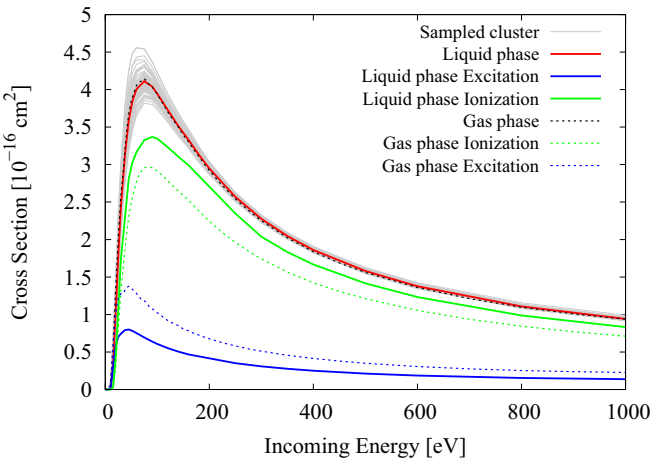

FIG. 4. Total IES CS for individual, randomly oriented water clusters (gray lines), averaged over all clusters (red line), and total IES CS for an isolated water molecule (dashed black line). Also shown are the excitation (blue) and ionization (green) contributions of the IES CS for liquid water (solid) and an isolated water molecule (dashed).

accounts for the sampling of the initial projectile direction. For comparison, the total CS for an isolated water molecule is shown (dashed black). As one can see, despite the considerable fluctuation in the total CS (in particular, for projectile energies below 200 eV) due to structural variations of the solvation cage, the total CS for inelastic collisions in liquid water seems, on average, almost identical to the one for an isolated water molecule [24–26]. However, our results show a significant enhancement of collisional ionization in the liquid. Indeed, the IES CS corresponding to collisional ionization is at its maximum almost 15% higher in the liquid (solid green) than for an isolated water molecule (dashed green). On the other hand, the excitation contribution is considerably decreased in the liquid environment (solid blue) in comparison to the isolated molecule (dashed blue) by more than 40% at its peak value. This reveals a substantial difference between the scattering by an isolated molecule and a molecule in a liquid environment.

In Fig. 5, we show the IES CS decomposed into MO-resolved contributions, i.e., only accounting for the formation of a hole (mostly) localized on a given orbital. The results show noticeable differences between the liquid environment and the isolated molecule. The MO-resolved CSs all increase relatively quickly starting at the first electronic excitation energy for the respective hole. For each hole type, a slightly different maximum is reached, followed by a smooth decay with increasing projectile energy.

As can be seen, neither in the liquid environment nor for the isolated molecule do our calculations indicate any strong preference in terms of hole creation in any of the three outermost $1b_1$, $3a_1$, and $1b_2$ orbitals. Also, in both cases the IES CS involving the inner $2a_1$ orbital is always notably weaker. Remarkably, the relative ordering of the CS involving the outermost electrons is different for isolated water and for water in the liquid environment. Specifically, for the liquid case, at projectile energies around 300 eV, the partial cross section for a hole in the $1b_2$ orbital is around 10% larger than for a hole

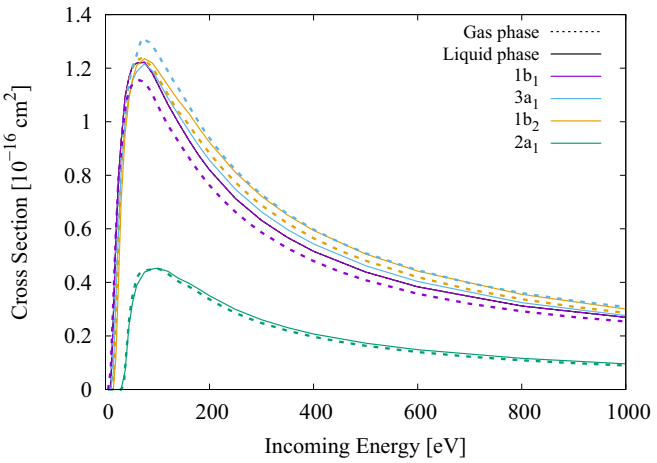

FIG. 5. MO-resolved IES CSs for an isolated water molecule (dashed line) and for a water molecule in the liquid phase (solid line).

in the $3a_1$ orbital and 15% larger than for a hole in the $1b_1$ orbital. For the isolated water molecule, in contrast, the CS is the largest for a hole in the $3a_1$ orbital, which is about 5% larger than the CS for a hole in the $1b_2$ orbital and more than 20% larger than for a hole in the $1b_1$ orbital. It is noted that a contrasting picture is observed at very low projectile energy due to the difference in first excitation and binding energies of these individual electrons.

The IES CSs involving the $1b_1$ and $1b_2$ orbitals, respectively, increase by about 7% and 4% due to the liquid environment, whereas the IES CS for the $3a_1$ orbital is decreased by about 9%. Interestingly, both $1b_1$ and $1b_2$ orbitals display polarization along the hydrogen bonds formed in the liquid.

In order to explore these trends, the electron-density differences associated with the occupied (localized and recanonicalized) orbitals centered on the central water molecule of a paradigm water pentamer and those of an isolated water molecule are depicted in Fig. 6. As one can see, the electron density associated with the $1b_1$ orbital increases in the pentamer along the directions pointing toward the (not depicted) two hydrogen-bond donor solvent molecules and decreases in the vicinity of the central oxygen atom. In the case of the $1b_2$ orbital, the liquid environment induces a polarization along the intramolecular OH bonds, leading to a local increase of the electron density in the vicinity of the central oxygen atom and a reduction of the electron density around the hydrogen atoms, i.e., in the direction of the hydrogen-bond acceptor solvent molecules. In contrast, polarization of the $3a_1$ orbital occurs mostly along the symmetry axis of the water molecule. Finally, the polarization of the inner $2a_1$ orbital is more localized in the direct vicinity of the water molecule and appears to be mostly occurring through a slight mixing with the initial $3a_1$ orbital. Quantitatively, these polarization effects displace about 2%, 4%, 3%, and 2%, respectively, of the electron density associated with the gas-phase $1b_1$, $3a_1$, $1b_2$, and $2a_1$ orbitals.

Moreover, we compare the IPs for water in the liquid environment and isolated water in Table I, as obtained from our calculation. As can be seen, polarization of the occupied MOs of water due to the interaction with the solvating molecules in the liquid leads to a slight decrease in IP for all the valence

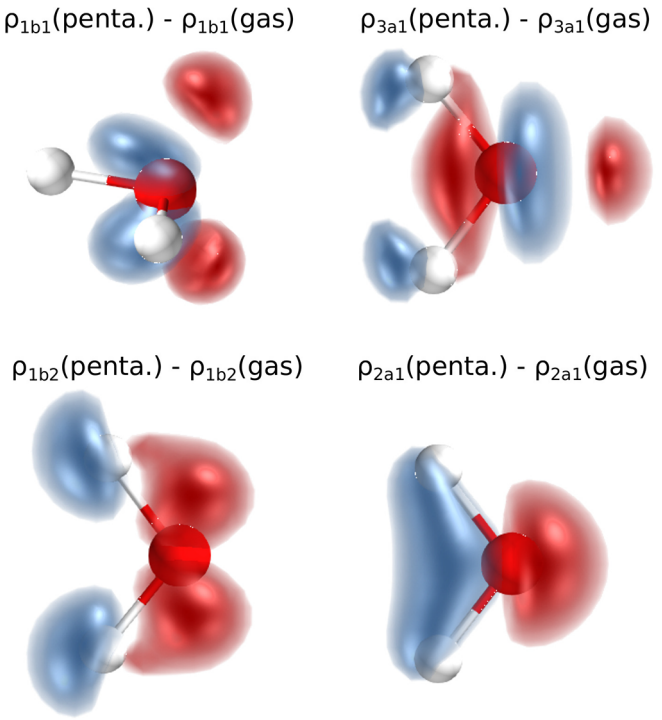

FIG. 6. Difference of electron density between the (recanonicalized localized) occupied orbitals centered on the central water molecule of a paradigm water pentamer and those of a gas-phase water molecule. Red areas indicate an increase in electron density in the pentamer, whereas blue regions indicate a decrease. Contour value used in the plot: 0.001.

orbitals in comparison to an isolated molecule. Notably, in reality, the IP of liquid water is lower and shows a much stronger difference to the one for the isolated molecule due to the dynamic polarization effect of the surrounding water molecules, which is not considered in the calculations.

Overall, the reported changes in the electron densities and the IPs are rather small and can likely not explain the rather dramatic change of ionization versus excitation contributions reported in Fig. 4. Instead, we can see that the computed lowest excitation energies also reported in Table I show a much stronger solvation effect, pointing toward the fact that the impact of the solvation on the IES is much more due to the wave function of the excited or released electron in the final state. This can be linked to the fact that the repulsive environment induced by the neighboring water molecules in the liquid phase prevents the existence of a series of excited Rydberg states.

TABLE I. Computed Koopmans' ionization potentials and excitation energies (in eV) for electrons in the four outermost orbitals of an isolated water molecule and those of liquid water.

	$1b_1$	$3a_1$	$1b_2$	$2a_1$
IP: gas	13.90	15.94	19.66	36.97
IP: liquid	13.77	15.73	18.93	36.11
E_{ex}: gas	8.74	10.94	14.48	31.91
E_{ex}: liquid	10.15	12.52	15.51	33.02

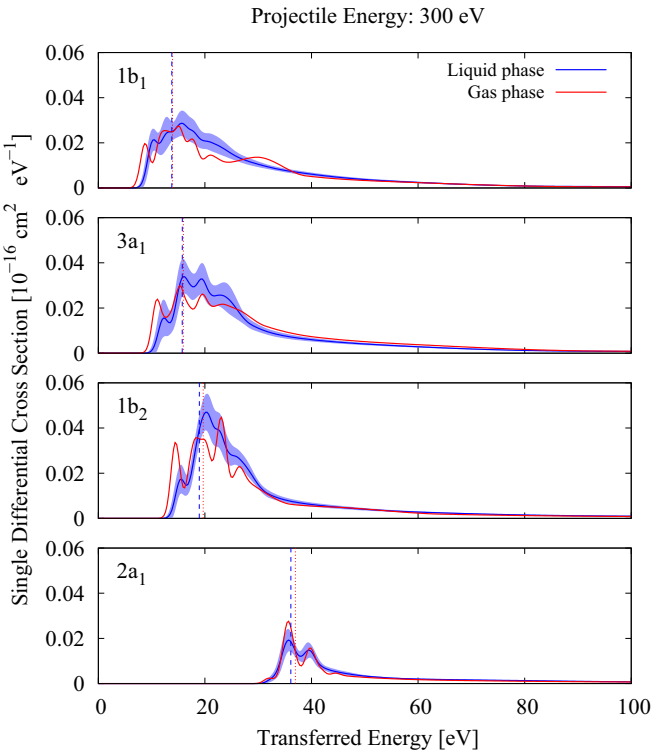

FIG. 7. MO-resolved IES SDCS for an isolated water molecule (red) and a water molecule in liquid environment (blue), for an electron projectile energy of 300 eV. The blue shade indicates cross-section variations of up to one standard deviation of the SDCS distribution across the set of sampled clusters. For the isolated molecule, bound transitions were broadened using a Gaussian profile of 2.0 eV full width at half maximum (FWHM), whereas the ionization continua were reconstructed from the pseudocontinuum transitions using the Stieltjes-imaging procedure. Vertical bars indicate the IPs of the corresponding orbitals for water in the liquid (dashed blue) and for an isolated water molecule (dotted red).

2. *Energy-resolved inelastic electron scattering*

To identify further differences between the IES for an isolated water and for liquid water, we investigate the SDCS resolving the probability of any given amount of energy to be transferred from the projectile to the target. In Fig. 7, MO-resolved SDCSs are reported for isolated water and water in liquid environment considering a projectile energy of 300 eV.

Low-energy features of the IES SDCS correspond to bound-to-bound excitations and are less sharp for the liquid water due to the extra broadening stemming from structural variations. In Fig. 7, changes in SDCS due to fluctuation of the local environment in the liquid are depicted by the blue shaded areas (standard deviations). In the region of larger transferred energy, i.e., in the region describing the ejection of a secondary electron with sufficiently large kinetic energy, these structural fluctuations have almost no impact on the collision, so variations of the SDCSs at transferred energies above 50 eV are very small.

Comparing the results for liquid water with those for an isolated water molecule, one observes that, for the $1b_1$, $3a_1$, and $1b_2$ orbitals in liquid water, the onset of the IES SDCS is slightly shifted toward higher transferred energy. This effect reflects the fact that the first excitation energy is generally larger for the molecule in the liquid environment than for the isolated molecule (see Table I). Overall, due to these shifts in the excitation energy, the IES SDCS is at these low transferred energies consistently smaller for the molecule in the liquid environment than for the isolated molecule, for all the outer bound molecular orbitals. At transferred energies above the ionization threshold (dashed and dotted lines), the IES SDCS is, in contrast, generally somewhat larger for the liquid than for the isolated molecule. Remarkably, the effects of the liquid environment on the IES are clearly beyond a global energy shift. Overall, we see that for each individual orbital, excitation and ionization contributions are altered considerably. The changes compensate each other in a way that the differences in the total scattering cross section are rather small.

From the perspective of a projectile electron with a kinetic energy around 300 eV, the liquid-environment-induced changes imply a trend toward a somewhat larger energy loss that overall does not seem very dramatic. For simulating scattering dynamics, however, it is crucial whether the target molecule is excited or ionized and to what degree low-energy electrons are released through collisional ionization, since they can cause further IES events.

To go toward the simulation of the collisional-cascade dynamics, the characteristics of IES need to be described over a large collision-energy window, because in each collision that incident projectile electron loses part of its energy. Thus, as a final result, we report the complete scan of the IES SDCS for liquid water for projectile energies up to 1000 eV. In Fig. 8(a), the IES SDCS is reported as a function of projectile energy and transferred energy. Such a map illustrates the perspective of the projectile electron, displaying how much energy it loses in each collision. Across the range of collision energies investigated, the IES CS is strongest for transferred energies between ca. 10 and 45 eV. This energy range corresponds to bound-to-bound excitations as well as ionization into the low-energy continuum. Scattering events involving the creation of a hole in one of the three outermost $1b_1$, $3a_1$, and $1b_2$ orbitals materialize as the region of very large SDCS at transferred energies between 10 and 30 eV, whereas collisions involving the deeper $2a_1$ orbital are responsible for the weaker structures between 35 and 45 eV.

In Fig. 8(b), the molecular aspect of IES is highlighted in the structure of the SDCS. Here, we show the SDCS as a function of the projectile energy and the energy actually deposited in the molecular target, i.e., not accounting for the energy transferred to the ejected electron in case of collisional ionization. In this representation, the SDCS clearly displays four excitation bands, each corresponding to one of the four outermost occupied orbitals of the target water molecule and converging to their corresponding IP.

Finally, in Fig. 8(c), we relate the IES SDCS to the behavior of the electrons in the target. In this representation, the SDCS is plotted as a function of the projectile energy and the energy of the excited/ejected electron. A negative energy indicates that the target becomes electronically excited, whereas positive energies indicate ionization and represent the kinetic energy of the released secondary electron. From such a picture, one can clearly observe that collisional ionization dominates the IES process at almost every projectile energy.

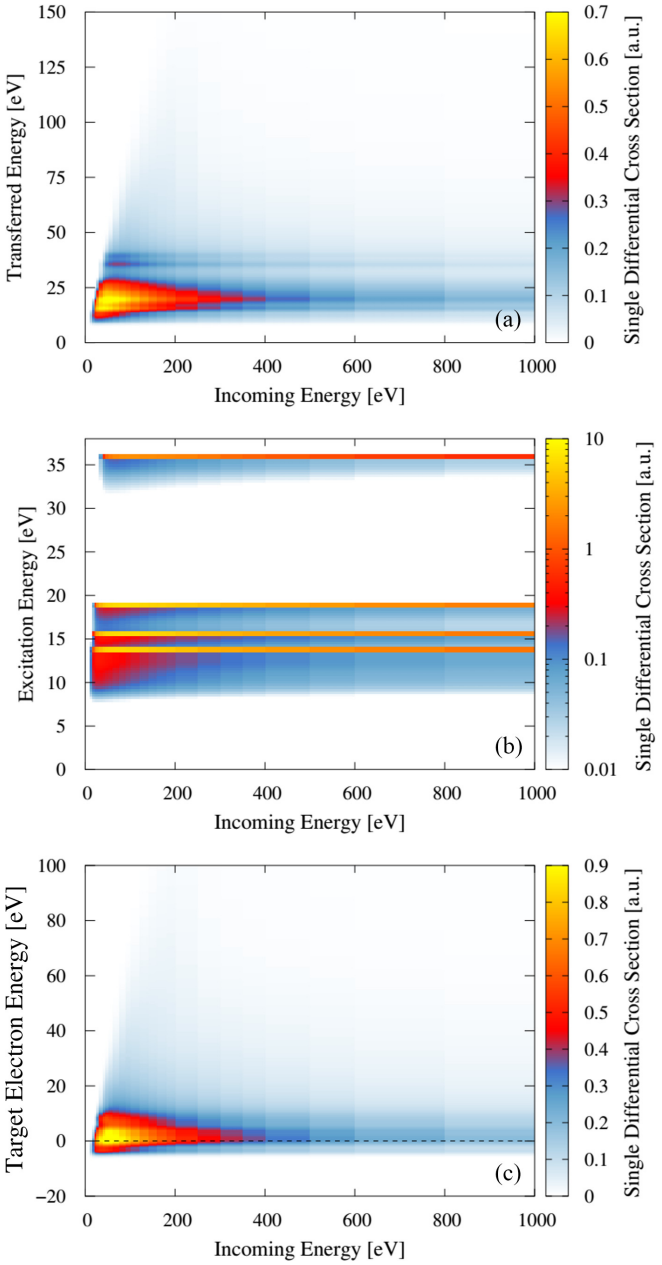

FIG. 8. IES SDCS of liquid-phase water as a function of the incoming electron energy and (a) the energy transferred from the projectile to the scattering target; (b) the energy deposited in the molecular target; and (c) the final energy of the excited or ejected electron. Results were averaged over the 50 randomly sampled clusters. Bound transitions were broadened using a Gaussian profile of 2.0 eV FWHM, whereas the ionization continua were reconstructed from the pseudocontinuum transitions using Stieltjes' imaging.

Secondary electrons are most likely ejected with a kinetic energy below 20 eV. In particular, at collision energy greater than 200 eV, emission of such slow secondary electrons captures about 65% of the collisional ionization CS. The fraction of low-energy electrons (kinetic energy below 20 eV) greatly increases with lower impact energy (about 75% at 100 eV and more than 90% below 50 eV).

IV. CONCLUSION

In this paper, we present an approach to computing inelastic electron-scattering cross sections in condensed phase and apply it to liquid water. Our method is based on a pseudocontinuum approach to describe ionization, allowing the final state of the system to be described in the framework of standard quantum-chemistry methods. We emphasize the molecular aspect of the process by resolving individual excitation channels as well as the transition from the excitation to the ionization regime. This contrasts with other methods that focus purely on electron-impact-induced ionization events by employing a continuum wave for the description of the final state of the target. These approaches cannot be straightforwardly applied to condensed-phase systems. In contrast, our approach provides a path toward a description of IES events with molecular-hole-state resolution that is more naturally applicable to the condensed phase.

For isolated water molecules, our calculation results show good agreement with measured ionization cross sections. For liquid-phase calculations, we computed total and hole-resolved single differential cross sections for the IES process, drawing a full molecular picture of IES events in this medium.

A comparison reveals differences between liquid-phase and gas-phase IES cross sections. Specifically, we find that electron-impact-induced excitation is suppressed in the liquid. This is compensated by a larger impact-induced ionization CS. Overall, these effects compensate each other in the total (i.e., excitation and ionization) IES cross section. For the hole-resolved total IES cross section, we find differences between the liquid phase and the gas phase below 10%.

The observed changes are shown to stem from nontrivial modifications of the IES single differential cross sections in the liquid and are expected to have considerable impact for the modeling of ionization cascades in liquid water: Since the liquid environment enhances the electron-impact-induced ionization CS, considerably more secondary electrons are released than one would expect from the CS computed for isolated water molecules.

ACKNOWLEDGMENTS

We acknowledge support from DESY (Hamburg, Germany), a member of the Helmholtz Association (HGF). L.I. and R.S. further acknowledge support from the Cluster of Excellence "CUI: Advanced Imaging of Matter" of the Deutsche Forschungsgemeinschaft (DFG)—EXC 2056—Project ID 390715994. The authors acknowledge the scientific exchanges and support of the Center for Molecular Water Science (CMWS).

DATA AVAILABILITY

The data that support the findings of this article are not publicly available. The data are available from the authors upon reasonable request.

APPENDIX A: RESTRICTED CIS FOR IES CLUSTER CALCULATIONS

In this Appendix, we assess the effect of restricting the CIS calculation to only single excitations involving electrons

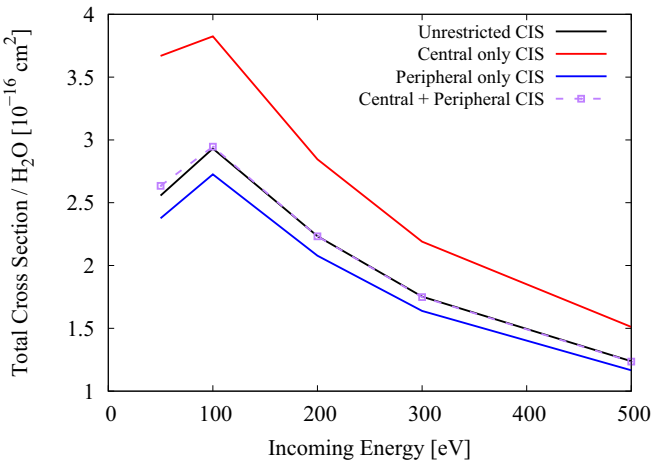

FIG. 9. Total inelastic scattering CS per scattering molecule for an isolated tetrahedral water cluster $(H_2O)_5$ computed at the CIS level. (Black) Including all possible single excitations. (Red) Including only single excitations from MOs localized on the central molecule. (Blue) Including only single excitations from MOs localized on a peripheral water molecule. (Dashed purple) Weighted average of central and peripheral contributions.

localized on the central water molecule of a cluster. To do so, we computed the IES total cross section for a prototypical tetrahedral water pentamer with and without applying such a restriction. For the IES calculation, we proceeded following the same approach as described in the main body of this article but we also performed the recanonicalization procedure for the four peripheral water molecules.

In Fig. 9, we report the total IES CS per water molecule computed from the full pentamer, i.e., including single excitations from all occupied valence orbitals (black) as well as from the central water molecule only (red) and from the four peripheral water molecules (blue). As one can see, the CS obtained from the restricted calculations (dotted purple) is almost identical as performing the full cluster calculation. This shows that the description of IES is not biased by decoupling the various scattering centers from each other.

In the liquid, every water molecule should be indistinguishable from any other water molecule up to the fluctuations of their local environment. However, in the present cluster calculation, it is clear that the peripheral molecules behave differently than the central one. These differences can be in part attributed to the differentiated treatment of their respective electronic structure due to the basis set favoring the central water molecule through the complementary Kaufmann functions. However, the main source of physical discrepancies between central and peripheral water molecules in our cluster calculation is the incomplete solvation shell experienced by the molecules at the boundary of the quantum mechanical region; only the central water molecule in the cluster experiences a true liquidlike environment. We thus stress that this decoupling is not a mere computational trick but a critical step to isolate the physical contributions of the central water molecule.

To further evaluate the quality of the description of the electronic structure of the target, we present in Fig. 10 the

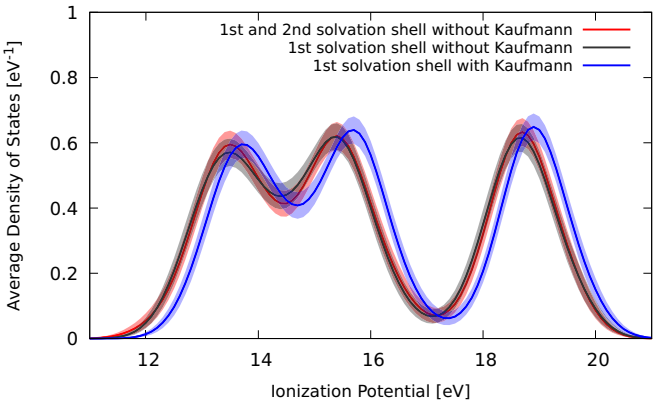

FIG. 10. Density of cationic states for the central water molecule computed at the one-hole CI level for various basis sets and QM regions (see text) considering the 50 sampled water clusters. Individual state contributions were convolved with a Gaussian profile of 1 eV FWHM. The shaded area shows the standard error due to finite sampling.

density of cationic states for the central water molecule. These were computed at the one-hole–configuration-interaction level including as explicit molecules in the quantum calculation either only the water molecules up to the first solvation shell (as in the main body of this paper) or by including 16 water molecules, i.e., up to the second solvation shell. We also investigated the influence of adding Kaufmann basis functions to the basis set of the central O atom. As can be seen, inclusion of the second solvation shell in our model has no noticeable effect on the density of hole states, whereas the Kaufmann basis functions induce a sub-eV shift of the different peaks. A comparison with photoelectron spectra of liquid water [62] reveals that while the $1b_1$ peak width is in agreement with our simulated density of states, our model underestimates the broadening of the $3a_1$ and $1b_2$ peaks. This behavior is likely caused by the freezing of the internal degrees of freedom of the individual water molecules in our cluster sampling procedure.

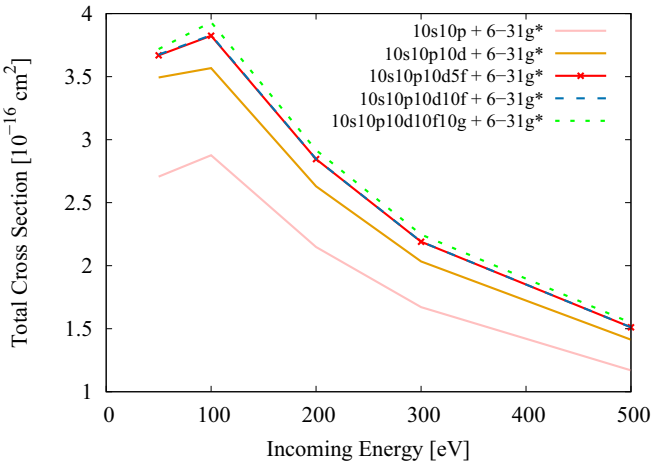

FIG. 11. Convergence of the total IES CS with respect to the size of the basis set for the water molecule in the center of an optimized tetrahedral water pentamer.

APPENDIX B: BASIS-SET CONVERGENCE OF CLUSTER CALCULATIONS

In Fig. 11, we report a basis-set convergence test for the cluster calculation. The total IES CS was computed for the central molecule of an optimized tetrahedral water pentamer for different basis sets. As can be seen, a similar behavior is observed as for the isolated water molecule; i.e., convergence is reached for the 6−31G* basis supplemented with 10*s*, 10*p*, 10*d*, and 5*f* Kaufmann functions.

[1] S. Li *et al.*, Attosecond-pump attosecond-probe x-ray spectroscopy of liquid water, Science **383**, 1118 (2024).

[2] D. K. Jain and S. P. Khare, Ionizing collisions of electrons with CO_2, CO, H_2O, CH_4 and NH_3, J. Phys. B: At. Mol. Phys. **9**, 1429 (1976).

[3] Y.-K. Kim and M. E. Rudd, Binary encounter dipole model for electron-impact ionization, Phys. Rev. A **50**, 3954 (1994).

[4] W. Hwang, Y.-K. Kim, and M. E. Rudd, New model for electron-impact ionization cross sections of molecules, J. Chem. Phys. **104**, 2956 (1996).

[5] S. Pal, M. Kumar, R. Singh, and N. Kumar, Evaluation of electron-impact ionization cross sections for molecules, J. Phys. Chem. A **123**, 4314 (2019).

[6] M. Luthra, K. Goswami, A. K. Arora, A. Bharadvaja, and K. L. Baluja, Mass spectrometry-based approach to compute electron-impact partial ionization cross-sections of methane, water and nitromethane from threshold to 5 keV, Atoms **10**, 74 (2022).

[7] D. Emfietzoglou, Inelastic cross-sections for electron transport in liquid water: A comparison of dielectric models, Radiat. Phys. Chem. **66**, 373 (2003).

[8] D. Emfietzoglou, F. A. Cucinotta, and H. Nikjoo, A complete dielectric response model for liquid water: A solution of the Bethe ridge problem, Radiat. Res. **164**, 202 (2005).

[9] H. Date, K. L. Sutherland, H. Hasegawa, and M. Shimozuma, Ionization and excitation collision processes of electrons in liquid water, Nucl. Instrum. Methods Phys. Res. Sect. B **265**, 515 (2007).

[10] H. Shinotsuka, B. Da, S. Tanuma, H. Yoshikawa, C. J. Powell, and D. R. Penn, Calculations of electron inelastic mean free paths. XI. Data for liquid water for energies from 50 eV to 30 keV, Surf. Interface Anal. **49**, 238 (2017).

[11] A. Schild, M. Peper, C. Perry, D. Rattenbacher, and H. J. Wörner, Alternative approach for the determination of mean free paths of electron scattering in liquid water based on experimental data, J. Phys. Chem. Lett. **11**, 1128 (2020).

[12] R. Signorell, Electron scattering in liquid water and amorphous ice: A striking resemblance, Phys. Rev. Lett. **124**, 205501 (2020).

[13] N. Sinha and B. Antony, Mean free paths and cross sections for electron scattering from liquid water, J. Phys. Chem. B **125**, 5479 (2021).

[14] N. E. Koval, P. Koval, F. Da Pieve, J. Kohanoff, E. Artacho, and D. Emfietzoglou, Inelastic scattering of electrons in water from first principles: Cross sections and inelastic mean free path for use in Monte Carlo track-structure simulations of biological damage, R. Soc. Open Sci. **9**, 212011 (2022).

[15] K. A. Long, H. G. Paretzke, F. Müller-Plathe, and G. H. F. Diercksen, Calculation of double differential cross sections for the interaction of electrons with a water molecule, clusters of water molecules, and liquid water, J. Chem. Phys. **91**, 1569 (1989).

[16] C. Champion, J. Hanssen, and P. A. Hervieux, Electron impact ionization of water molecule, J. Chem. Phys. **117**, 197 (2002).

[17] S. Houamer, C. Dal Cappello, and A. Mansouri, Differential and total cross sections for the ionization of water molecule by electron impact, J. Electron Spectrosc. Relat. Phenom. **161**, 38 (2007).

[18] I. Tóth, R. I. Campeanu, V. Chiş, and L. Nagy, Electron impact ionization of diatomic molecules, Eur. Phys. J. D **48**, 351 (2008).

[19] I. Tóth, R. I. Campeanu, V. Chiş, and L. Nagy, Ionization of the water molecule by electron and positron impact, J. Phys.: Conf. Ser. **199**, 012018 (2010).

[20] C. Champion, Theoretical cross sections for electron collisions in water: Structure of electron tracks, Phys. Med. Biol. **48**, 2147 (2003).

[21] C. F. Perry, P. Zhang, F. B. Nunes, I. Jordan, A. von Conta, and H. J. Wörner, Ionization energy of liquid water revisited, J. Phys. Chem. Lett. **11**, 1789 (2020).

[22] V. Ziaei and T. Bredow, Red and blue shift of liquid water's excited states: A many body perturbation study, J. Chem. Phys. **145**, 064508 (2016).

[23] H. Tsuchida, T. Tezuka, T. Kai, Y. Matsuya, T. Majima, and M. Saito, Liquid water radiolysis induced by secondary electrons generated from MeV-energy carbon ions, J. Chem. Phys. **161**, 104503 (2024).

[24] M. L. de Sanctis, M.-F. Politis, R. Vuilleumier, C. R. Stia, and O. A. Fojón, Liquid water ionization by fast electron impact: A multiple differential study for the $1B_1$ orbital, J. Phys. B: At. Mol. Opt. Phys. **45**, 045206 (2012).

[25] M. L. de Sanctis, M.-F. Politis, R. Vuilleumier, C. R. Stia, and O. A. Fojón, Theoretical study of the ionization of liquid water from its several initial orbitals by fast electron impact, J. Phys. B: At. Mol. Opt. Phys. **48**, 155201 (2015).

[26] M. L. de Sanctis, M.-F. Politis, R. Vuilleumier, C. R. Stia, and O. A. Fojón, Double differential cross sections for liquid water ionization by fast electron impact, Eur. Phys. J. D **71**, 125 (2017).

[27] W. P. Reinhardt, L^2 discretization of atomic and molecular electronic continua: Moment, quadrature and *J*-matrix techniques, Comput. Phys. Commun. **17**, 1 (1979).

[28] F. Müller-Plathe and G. H. F. Diercksen, Molecular photoionisation cross sections by moment theory. An introduction, in *Electronic Structure of Atoms Molecules and Solids, Proceedings of the II Escola Brasileira de Estruture Eletronica, Olinda, Brazil*, 1989, edited by S. Canuto, J. D'Albuquerque e Castro, and F. J. Paixao (World Scientific, Singapore, 1990), pp. 1–29.

[29] J. J. Bekx, S.-K. Son, R. Santra, and B. Ziaja, *Ab initio* calculation of electron-impact-ionization cross sections for ions in exotic electron configurations, Phys. Rev. A **98**, 022701 (2018).

[30] M. C. Zammit, D. V. Fursa, J. S. Savage, and I. Bray, Electron- and positron- molecule scattering: Development of the molecular convergent close-coupling method, J. Phys. B: At. Mol. Opt. Phys. **50**, 123001 (2017).

[31] M. Ayouz, A. Faure, and V. Kokoouline, Theoretical study of the electron-induced vibrational excitation of H_2O, Astron. Astrophys. **687**, A3 (2024).

[32] K. Sturm, Dynamic structure factor: An introduction, Z. Naturforsch. A **48**, 233 (1993).

[33] M. Inokuti, Inelastic collision of fast charged particles with atoms and molecules—The Bethe theory revisited, Rev. Mod. Phys. **43**, 297 (1971).

[34] J. Kirschner, Direct and exchange contributions in inelastic scattering of spin-polarized electrons from iron, Phys. Rev. Lett. **55**, 973 (1985).

[35] M. Shorifuddoza, M. H. Khandker, G. B. Ragimkhanov, Z. R. Khalikova, P. K. Das, H. Watabe, A. K. F. Haque, and M. A. Uddin, Electron and positron scattering by water molecules: Cross sections and transport characteristics, Eur. Phys. J. D **79**, 62 (2025).

[36] M. J. Abraham, T. Murtola, R. Schulz, S. Páll, J. C. Smith, B. Hess, and E. Lindahl, GROMACS: High performance molecular simulations through multi-level parallelism from laptops to supercomputers, SoftwareX **1–2**, 19 (2015).

[37] H. J. C. Berendsen, J. R. Grigera, and T. P. Straatsma, The missing term in effective pair potentials, J. Phys. Chem. **91**, 6269 (1987).

[38] W. L. Jorgensen, D. S. Maxwell, and J. Tirado-Rives, Development and testing of the OPLS all-atom force field on conformational energetics and properties of organic liquids, J. Am. Chem. Soc. **118**, 11225 (1996).

[39] G. Bussi, D. Donadio, and M. Parrinello, Canonical sampling through velocity rescaling, J. Chem. Phys. **126**, 014101 (2007).

[40] M. Parrinello and A. Rahman, Crystal structure and pair potentials: A molecular-dynamics study, Phys. Rev. Lett. **45**, 1196 (1980).

[41] M. Parrinello and A. Rahman, Polymorphic transitions in single crystals: A new molecular dynamics method, J. Appl. Phys. **52**, 7182 (1981).

[42] J. R. Ray and A. Rahman, Statistical ensembles and molecular dynamics studies of anisotropic solids, J. Chem. Phys. **80**, 4423 (1984).

[43] P. P. Ewald, Die berechnung optischer und elektrostatischer gitterpotentiale, Ann. Phys. (NY) **369**, 253 (1921).

[44] T. Darden, D. York, and L. Pedersen, Particle mesh Ewald: An $N \cdot \log(N)$ method for Ewald sums in large systems, J. Chem. Phys. **98**, 10089 (1993).

[45] J. Wang, G. Román-Pérez, J. M. Soler, E. Artacho, and M.-V. Fernández-Serra, Density, structure, and dynamics of water: The effect of van der Waals interactions, J. Chem. Phys. **134**, 024516 (2011).

[46] K. Kaufmann, W. Baumeister, and M. Jungen, Universal Gaussian basis sets for an optimum representation of Rydberg and continuum wavefunctions, J. Phys. B: At. Mol. Opt. Phys. **22**, 2223 (1989).

[47] E. Coccia, B. Mussard, M. Labeye, J. Caillat, R. Taïeb, J. Toulouse, and E. Luppi, Gaussian continuum basis functions for calculating high-harmonic generation spectra, Int. J. Quantum Chem. **116**, 1120 (2016).

[48] R. Ditchfield, W. J. Hehre, and J. A. Pople, Self-consistent molecular-orbital methods. IX. An extended Gaussian-type basis for molecular-orbital studies of organic molecules, J. Chem. Phys. **54**, 724 (1971).

[49] W. J. Hehre, R. Ditchfield, and J. A. Pople, Self-consistent molecular orbital methods. XII. Further extensions of Gaussian-type basis sets for use in molecular orbital studies of organic molecules, J. Chem. Phys. **56**, 2257 (1972).

[50] P. C. Hariharan and J. A. Pople, The influence of polarization functions on molecular orbital hydrogenation energies, Theor. Chim. Acta **28**, 213 (1973).

[51] S. F. Boys, Construction of some molecular orbitals to be approximately invariant for changes from one molecule to another, Rev. Mod. Phys. **32**, 296 (1960).

[52] J. M. Foster and S. F. Boys, Canonical configurational interaction procedure, Rev. Mod. Phys. **32**, 300 (1960).

[53] R. Vuilleumier and M. Sprik, Electronic properties of hard and soft ions in solution: Aqueous Na^+ and Ag^+ compared, J. Chem. Phys. **115**, 3454 (2001).

[54] Y. Hao, L. Inhester, K. Hanasaki, S.-K. Son, and R. Santra, Efficient electronic structure calculation for molecular ionization dynamics at high x-ray intensity, Struct. Dyn. **2**, 041707 (2015).

[55] L. Inhester, K. Hanasaki, Y. Hao, S.-K. Son, and R. Santra, X-ray multiphoton ionization dynamics of a water molecule irradiated by an x-ray free-electron laser pulse, Phys. Rev. A **94**, 023422 (2016).

[56] Q. Sun, T. C. Berkelbach, J. D. McClain, and G. K.-L. Chan, Gaussian and plane-wave mixed density fitting for periodic systems, J. Chem. Phys. **147**, 164119 (2017).

[57] V. I. Lebedev and D. N. Laikov, A quadrature formula for the sphere of the 131st algebraic order of accuracy, Dokl. Math. **59**, 477 (1999).

[58] J. Schutten, F. J. de Heer, H. R. Moustafa, A. J. H. Boerboom, and J. Kistemaker, Gross- and partial-ionization cross sections for electrons on water vapor in the energy range 0.1–20 keV, J. Chem. Phys. **44**, 3924 (1966).

[59] M. A. Bolorizadeh and M. E. Rudd, Angular and energy dependence of cross sections for ejection of electrons from water vapor. I. 50–2000 eV electron impact, Phys. Rev. A **33**, 882 (1986).

[60] N. L. Djurić, I. M. Čadež, and M. V. Kurepa, H_2O and D_2O total ionization cross-seciions by electron impact, Int. J. Mass Spectrom. Ion Processes **83**, R7 (1988).

[61] H. C. Straub, B. G. Lindsay, K. A. Smith, and R. F. Stebbings, Absolute partial cross sections for electron-impact ionization of H_2O and D_2O from threshold to 1000 eV, J. Chem. Phys. **108**, 109 (1998).

[62] D. Nordlund, M. Odelius, H. Bluhm, H. Ogasawara, L. Pettersson, and A. Nilsson, Electronic structure effects in liquid water studied by photoelectron spectroscopy and density functional theory, Chem. Phys. Lett. **460**, 86 (2008).